Proceedings of the Combustion Institute 41 (2025) 105929

Contents lists available at ScienceDirect

Proceedings of the Combustion Institute

journal homepage: www.elsevier.com/locate/proci

A joint experimental and numerical study of multiple hydrogen flames in a jet in crossflow configuration

Preethi Rajendram Soundararajan [a,b,*], Pierre Q. Gauthier [c], Peter J. Benie [b], Epaminondas Mastorakos [b]

[a] Department of Aeronautics & Astronautics, University of Southampton, Southampton SO16 7QF, United Kingdom
[b] Department of Engineering, University of Cambridge, Cambridge, CB2 1PZ United Kingdom
[c] Siemens Energy, Montreal, Quebec H8T 3H1, Canada

ARTICLE INFO

Keywords:
Jet in crossflow
Hydrogen combustion
Large eddy simulation
Flame stabilisation

ABSTRACT

This work investigates multiple jets in crossflow (JICF) injection of hydrogen in a laboratory-scale canonical configuration in anticipation of the presence of this geometrical feature in future hydrogen gas turbine combustors. The experimental setup comprises a square cross-section plenum delivering a crossflow of air and a hydrogen injection plate delivering three hydrogen jets. To achieve a wide range of momentum flux ratios, three different injection plates with different hole diameters are employed for the hydrogen jets. In the first step, the schlieren technique is used to visualise the non-reacting flow with helium as a surrogate, followed by the study of pure hydrogen flames using OH* chemiluminescence. The flames exhibit different dynamical behaviour, including a partial flame lift-off on the windward side at the higher momentum flux ratio. To further understand the flame and flow behaviour, in the second step, large eddy simulations (LES) of the experimental configuration are performed, which effectively capture the experimental observations in terms of jet and flame shape. It is seen from experiments and LES that at the highest momentum flux ratio, the jet penetrates further into the chamber, with most of the mixing taking place within a short region downstream of the jet. This leads to a compact flame that is stabilised farther from the inner wall. However, the higher momentum carried by the jets results in less intense mixing near the exit, leading to partial flame lift-off. As the momentum flux ratio decreases, the penetration of the jet diminishes, leading to reduced mixing. The delayed mixing leads to a longer flame anchored at the injection location, close to the inner wall. The combined insights from experiments and LES at various momentum flux ratios have shed light on flame stabilisation mechanisms in JICF configurations, offering guidance for the development of hydrogen-based combustion systems.

1. Introduction

The growing need to tackle global warming has called for imminent steps to reduce the carbon emissions from air transport [1]. A proposed possibility is to use hydrogen as fuel, but hydrogen flames are generally prone to flashback, posing a safety concern when operated in premixed mode. To eliminate the above problem, it is necessary to achieve quick mixing of air and fuel directly in the combustion chamber and burn lean in order to reduce the formation of NO_x. One potential way to achieve this is to inject a high-velocity hydrogen jet into a crossflow (JICF) of air.

A JICF configuration typically consists of a jet with a velocity U_j issuing perpendicularly into crossflow with velocity U_∞. As outlined by Karagozian [2], such an arrangement is expected to feature a complex set of vortical structures, the most dominant being the counter-rotating vortex pair emanating at a certain distance in the jet injection section, which could enhance mixing properties [3,4]. In addition, horseshoe vortices would be formed due to the displacement of the crossflow field by the jet, wrapping the jet base in the boundary layer [3]. In a combustion environment, studying the interaction of these vortices with the flame is crucial. Such a flow field is typically characterised by the jet and crossflow velocities as well as their densities through a non-dimensional parameter called the momentum flux ratio J, which is defined as the ratio between the product of density (ρ_j) and square of velocity (U_j^2) of the jet to the product of density (ρ_∞) and square of the velocity (U_∞^2) of the crossflow [4], i.e., $J = \rho_j U_j^2 / \rho_\infty U_\infty^2$.

Huang and Wang [5] studied five different flow modes characterised by different momentum flux ratios for jet flames in a transverse air stream. As a general trend, it was found that for the low momentum

* Corresponding author at: Department of Aeronautics & Astronautics, University of Southampton, Southampton SO16 7QF, United Kingdom.
E-mail address: p.rajendram-soundararajan@soton.ac.uk (P. Rajendram Soundararajan).

https://doi.org/10.1016/j.proci.2025.105929
Received 14 July 2025; Accepted 25 September 2025
Available online 17 October 2025

Table 1
Summary of operating conditions and fluid properties considered in this work.

d_i (mm)	U_∞ (m s^{-1})	U_{jHe} (m s^{-1})	U_{jH_2} (m s^{-1})	J (–)	ϕ (–)	ρ_∞ (kg m^{-3})	ρ_{jHe} (kg m^{-3})	ρ_{jH_2} (kg m^{-3})
0.5		221	311	314				
0.7	4.6	113	159	82	0.1	1.29	0.18	0.09
1		55	78	20				

flux ratio cases, the flames were stabilised in the wake formed by the blockage of the tube. In cases with higher momentum flux ratios, entrainment by the high-velocity jet induces up-flow at the burner lip, thus preventing fuel from entering the wake region. Steinberg et al. [6] investigated hydrogen jet flames in a crossflow of preheated air at three different jet velocities using optical diagnostic tools. In all three cases, the authors found two flame branches, one stabilised on the leeward side and the other lifted along the windward side of the jet, with the branches connected together by a flame front covering the jet trajectory. The effect of jet injection angle on flame stabilisation in a hydrogen JICF configuration was investigated by Kolla et al. [7] using direct numerical simulation (DNS). For the same momentum flux ratio, it was found that reducing the jet injection angle from 90° to 75° destabilised the flame, resulting in a transient blowout. This behaviour was attributed to a kinematic imbalance between the flame propagation speed and the flow-normal velocity.

In a recent study, Saini et al. [8] investigated the flame-holding characteristics of hydrogen-enriched natural gas jet flames in crossflow. The study was conducted at a pressure of 10 bar with preheated air at various hydrogen enrichment levels. It was found that the level of enrichment modified the flame structure—while a higher enrichment resulted in the flames stabilising on both the windward and leeward side, a lower enrichment resulted in a flame stabilised only on the leeward side. Murugavel et al. [9] investigated the effect of pressure on mixing and combustion characteristics of a helium-diluted hydrogen jet using large eddy simulations (LES). They found that, at a fixed momentum flux ratio, increasing the pressure caused the lifted flame to attach to the nozzle as a result of the higher burning mass flux. Furthermore, their results showed that even in the case of a diluted hydrogen jet, the predominant combustion mode was premixed, with its contribution increasing with pressure.

From the literature study enumerated above, it is clear that the JICF configuration is suitable for stabilising pure hydrogen flames. Given the different flame stabilisation mechanisms produced by this configuration, it is instructive to understand the flow and flame dynamics at different values of its most influential parameter, which is the momentum flux ratio J. An important gap in the literature concerns the understanding of flame stabilisation through systematic variation of the momentum flux ratio. In addition, the interaction between multiple jets, which is expected to be used in practice, needs to be well understood. Thus, in this work, a canonical JICF configuration comprising three jets spaced at a fixed distance in a crossflow of air is developed. Holes of three different diameters are manufactured to achieve a broad range of momentum flux ratios. The ability to achieve wider ranges of the momentum flux ratio contributes to the development of a comprehensive dataset to close the existing gaps in the literature. Further details about the burner configuration and operating conditions are provided in the next section. This is followed by the results of the non-reactive flow visualisation measurements and reactive high-speed chemiluminescence imaging with hydrogen. The experiments are then compared against the LES of this test configuration. The results from LES help provide additional insights into the flow structures, enhancing the understanding of experimental observations and offering finer details that cannot be captured easily with experiments.

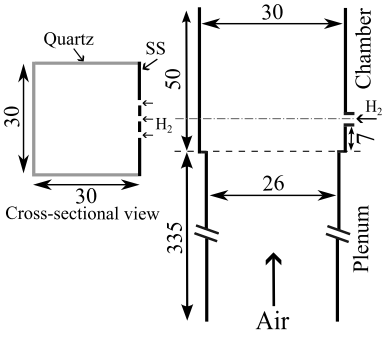

Fig. 1. Schematic of the jet in crossflow burner indicating critical dimensions in mm. Left: Cross-sectional view of the chamber showing the three injection holes. SS refers to stainless steel.

2. Experimental methods

2.1. Experimental setup

The experimental setup of the JICF burner configuration consists of a square cross-section settling chamber of dimensions 26 mm × 26 mm operating at atmospheric conditions. The square plenum of this combustor extends to 335 mm in length and leads to a square cross-section chamber of dimensions 30 mm × 30 mm where hydrogen is injected. The chamber has an optically accessible region made of quartz glass that is 25 mm wide and 50 mm high. A schematic of the experimental setup is presented in Fig. 1.

For hydrogen injection, a stainless steel (SS) plate is positioned on one side of the chamber with the three injection holes located at a height of 7 mm from the chamber inlet. The holes are distributed horizontally (perpendicular to crossflow direction) to ensure each flame experiences the same J. The spacing between the injection holes is fixed at 5 mm. Three hole diameters d_i = 0.5 mm, 0.7 mm and 1 mm are used in this study. The hydrogen injection plate comprises a small settling chamber at the back before the jet exits through the three injection holes to equalise the fluid flow through the three holes.

The air flow rate in these experiments is controlled by means of an *Alicat* mass flow controller having a full range of 2000 l$_s$/min. It has been shown that the jet trajectory in reactive flows closely follows the cold, non-reactive case [10]. Thus, as a first step, non-reactive characteristics of the flow field are examined using schlieren visualisation of helium jets, employed in place of hydrogen for safety reasons. A recent numerical study [11] further demonstrated that helium can serve as a surrogate for hydrogen, providing qualitative insight into global mixing parameters. The momentum flux ratio between the helium jet and the crossflow is maintained the same as that of a hydrogen jet in order to ensure a similar flow structure. In the second step, the combustor is ignited with hydrogen, and flame stabilisation at different operating conditions is visualised using high-speed chemiluminescence imaging. The jet flow is controlled through an *Alicat* mass flow meter having a full range of 50 l$_s$/min.

For the studies reported in this work, the velocity of air (crossflow) is maintained at U_∞ = 4.6 m s^{-1} (Re = 9900). A total jet flow rate of $\dot{q}_j$ = 11 l$_s$/min is chosen for hydrogen. This results in a per-jet momentum flux ratio of J = 314 at d_i = 0.5 mm, J = 82 at d_i = 0.7 mm, and J = 20 at d_i = 1 mm, with the flame operating at an overall equivalence ratio of ϕ = 0.1. A summary of the operating conditions, along with fluid properties, is provided in Table 1. A natural question might arise as to why the hole diameter is varied to obtain a change in the momentum flux ratio. This has been done to enable a wide variation in the momentum flux ratio (314 to 20), which is not commonly found in the literature with such configurations. The typical J values considered in the previous studies for reactive JICF studies are

between 10–30 [5,6,12,13] with the exception of [8], who have carried out measurements at $J = 106$ but at elevated pressure and temperature. Thus, in this study, a much higher momentum flux ratio and a wider range of momentum flux ratios ($J = 314, 82, 20$) are considered by using different injection hole diameters. Studies have also been conducted in the present configuration where the jet velocity is varied to modify the momentum flux ratio while maintaining the injection hole diameter and crossflow velocity constant. The corresponding results, shown in Fig. 3 of the Supplementary Material, exhibit the same behaviour as reported in the main text for a given hole diameter.

2.2. Methodology

For visualising the flow field, a schlieren arrangement that exploits the bending of light rays due to variations of density in the flow is employed. The light source is a Storz xenon lamp (model: NOVA 300) that is aperture-controlled (iris diaphragm D36S from *Thor Labs*) to provide a near-point source of light. First, a 500 mm focal length plano-convex lens (*Thor Labs*) converts the near-point light beam into parallel beams, which then pass through the JICF burner that forms the schlieren plane. The parallel light beam then passes through the second plano-convex lens (500 mm focal length from *Thor Labs*), which converges the parallel light beams onto a knife edge. The schlieren image is then captured by a *Photron* high-speed camera (model: Fastcam SA 1.1) operating at a gate width of ≈ 1.36 s, capturing 4000 frames per second. The images captured by the camera are background-subtracted to obtain the final schlieren images.

Next, to visualise the flame, high-speed chemiluminescence imaging is carried out to capture the light emission from OH^* radicals. Chemiluminescence originating from the excited radicals such as OH^* present in the flame zone has been demonstrated to be a measure of the rate of consumption of the combustible mixture, or in other words, the heat release rate for fully premixed flames [14]. More recently, Schiavone et al. [15] compared experimentally measured OH^* from a partially-premixed hydrogen combustor with LES-computed OH^* fields obtained by incorporating an OH^* sub-mechanism into the chemical kinetic scheme. Their results showed that OH^* fields not only agreed well between experiments and simulation, but also correlated reasonably with the LES-computed heat release rate field, even for the case of a diffusion hydrogen flame. Thus, in this work, OH^* chemiluminescence is used as a flame marker and is compared with the heat release rate field obtained from LES. The OH^* chemiluminescence is captured using a high-speed *Photron* CMOS camera (model: Fastcam SA 1.1) equipped with a narrow-band optical filter (*Edmund Optics*—50 mm diameter, hard coated, model: 34980) centred at 310±10 nm. The camera is fitted with a *LaVision* IRO intensifier unit (two-stage module with spectral range 190–800 nm) to amplify the OH^* signal and a *CERCO* 100 mm focal length UV-lens (F/2.8, model: 2178). The camera is operated at 4 kHz capturing 5457 frames of images in 1.36 s. The images are captured from two fields of view—one facing the injection holes, looking at the three jets from the front, and the other looking at the jets from the side, capturing the spatially integrated light intensity across the three jets. The side view, being line-of-sight integrated, inevitably blends the subtle differences between the three flames. It is worth noting that front-view schlieren visualisation, unlike OH^* chemiluminescence, is not feasible, as schlieren imaging requires optical access from two opposite sides of the chamber. In the present setup, the opaque SS plate used for hydrogen injection obstructs optical access on one side, and is an inherent experimental limitation for a front-view schlieren.

3. Experimental observations

3.1. Schlieren visualisation

Fig. 2 shows the different instantaneous schlieren images at the crossflow velocity of $U_\infty = 4.6\,\mathrm{m\,s^{-1}}$ for the three momentum flux ratios.

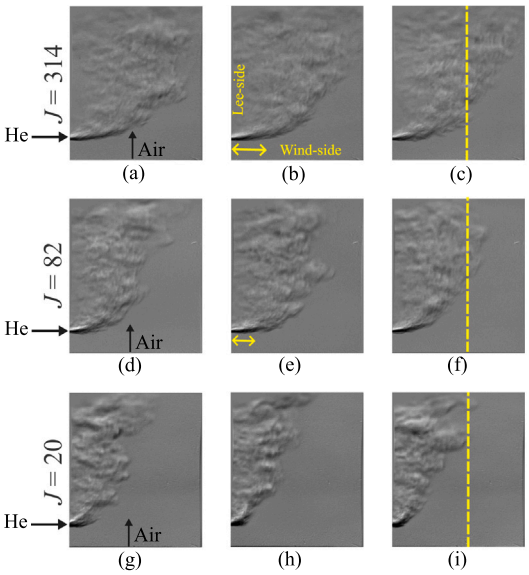

Fig. 2. Instantaneous schlieren images showing the visualisation of the helium jet in a crossflow of air under non-reactive conditions. Rows a–c correspond to $J = 314$, d–f correspond to $J = 82$, and g–i correspond to $J = 20$. The images in each column correspond to different instants in the acquisition window. The yellow vertical line corresponds to the limit of jet penetration at the lowest J, and the yellow arrow marks the jet stem.

These images provide a qualitative indication of the mixing between the jet and the crossflow. Firstly, it can be seen from the figure that the jet stem extends to a larger distance at a higher jet velocity. Here, the jet stem is defined as the straight portion of the jet before it bends and interacts with the crossflow and is marked with a yellow arrow in Fig. 2 (top row, middle image). However, this length decreases at $d_i = 0.7$ mm and nearly disappears at $d_i = 1$ mm with the vorticity sheet fully breaking the jet flow close to the injection location. It can also be seen that along the jet stem, on the windward side, the helium jet does not diffuse into the crossflow due to the higher momentum carried by the jet. On the other hand, along the leeward side, some diffusion of helium downstream into the chamber can be observed. It is also interesting to note that, at the higher momentum flux ratio (top row), along the inner wall (on the leeward side), there is an absence of jet penetration into the flow. On the other hand, as the momentum flux ratio decreases, the jet penetrates close to the inner wall (see bottom row) on the leeward side. This would result in wake vortices formed from the interaction of the jet with the boundary layer of the wall [16] contributing to the mixing between the jet and crossflow. The adherence of the jet to the wall has previously been observed at low momentum flux ratios [17,18] and is typically used in cooling applications [19].

The extent of jet penetration transversely into the chamber can be seen with the help of a dotted yellow vertical line (third column) marked on the images across the different momentum flux ratios. This dotted line marks the maximum spatial penetration of the jet at the lowest momentum flux ratio of $J = 20$. In comparison, the spatial jet penetration is increased by around 22% at the momentum flux ratio $J = 82$ and by 63% at $J = 314$ at a height of ≈ 25 mm from the jet inlet. Holdeman [20] had previously shown that jet penetration could be correlated with mixing. Hence, at $J = 314$, even though the mixing along the jet stem is nearly absent, good mixing between the jet and crossflow may be expected further downstream of the injection location. A similar trend has been observed earlier in [5] where the authors observed the down-wash area to increase with increasing momentum flux ratio. The degree of jet penetration into the crossflow can also be quantified by the jet angle relative to the jet axis. A shallower angle indicates stronger

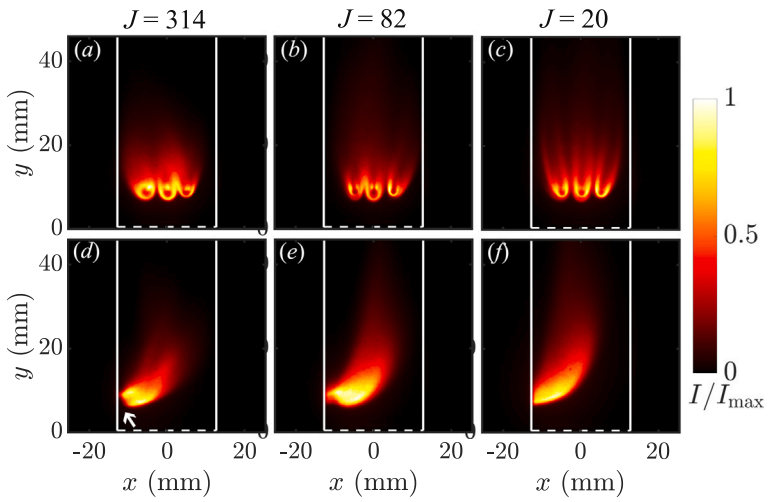

Fig. 3. Averaged OH* chemiluminescence intensity (line-of-sight integrated) captured from the flames showing the front view (a–c) and side view (d–f) of the jets. Images (a) & (d) are at $J = 314$, (b) & (e) are at $J = 82$, and (c) & (f) are at $J = 20$. The images are normalised by the maximum intensity and displayed in false colours. The solid white lines mark the limit of the chamber walls, and the dotted white line marks the chamber inlet. 0 on the x-axis corresponds to the centre of the burner.

transverse penetration and greater interaction with the crossflow, while a wider angle reflects the jet bending immediately upon injection. From the schlieren images, the jet angle is calculated to be 16° at $J = 340$, 18° at $J = 82$, and 31° at $J = 20$, indicating progressively weaker transverse penetration into the chamber with decreasing momentum flux ratio. Based on these observations, it can be expected that the best mixing between hydrogen and air under reactive conditions would happen at the highest momentum flux ratio, and the mixing is expected to gradually decline when moving to the lowest momentum flux ratio (bottom row). In the above analysis, only relative quantitative comparisons are presented, and hence, absolute uncertainties are not reported. To ensure the reliability and reproducibility of data, all experiments were carefully repeated under consistent conditions.

3.2. OH* chemiluminescence

Fig. 3 shows the front and side view of the averaged OH* chemiluminescence intensity (line-of-sight integrated) at the different momentum flux ratios in false colours. A video showing the transient flame behaviour is provided in the Supplementary Material, and the averaged images shown here retain the signature of the transient trends. The solid white vertical lines on the images mark the field of view of the camera in the chamber, and the dotted white horizontal line corresponds to the chamber inlet. It can be seen from Fig. 3 (top-left) that at the highest momentum flux ratio, the jets appear shorter but slightly broader, with the central jet having a preferential interaction with the right jet. The underlying reason for this preferential interaction remains unclear and will be investigated in future work, allowing the present study to maintain its focus on flame stabilisation. Each flame appears to have two segments—the outer flame having a 'U' shape that is open on the leeward side, and the second part of the flame appearing as a bright spot inside the 'U'. The reason for the flame having two segments can be appreciated from the side view of these jets shown in Fig. 3 (bottom-left). This image shows the integrated chemiluminescence intensity from the 3 jets (located one behind the other). It can be seen from this figure that the flame is lifted off from the injection location on the windward side (indicated by the white arrow) and remains slightly attached at the tip on the leeward side. This attached flame is visible in the front view as the small bright spot nearly at the centre of the 'U' shape.

At the momentum flux ratio of $J = 82$ (top-centre in Fig. 3), the flames are comparatively narrower and slightly longer than the flames at the highest J. The flames in this condition mostly only have a single segment with the 'U' shape. A minor lift-off tendency can be observed at the injection location in the form of a pinch-off on the windward side, but the flames are mostly stabilised at the injection location (see Fig. 3 bottom-centre). Unlike in the higher J case, the central flame appears to be nominally interacting with the left flame near the tip. At the lowest momentum flux ratio of $J = 20$ (Fig. 3 right), the flames are much longer and appear to broadly interact along the 'U' branch (red regions) with both the left and right flames (no preferential side). From Fig. 3 bottom-right, it can be seen that the flames are attached to the injection location, unlike the higher J cases. The flame angle relative to the inner wall is comparatively smaller, and this can be attributed to the jet bending shortly after entering the chamber at a lower momentum flux ratio, as seen in Fig. 2 (bottom row). From the side views, one can also observe that the high-intensity regions in the flame (inner flame brush marked by yellow and white regions) are longer at the lower momentum flux ratio.

In addition to the momentum flux ratios considered here, the jet velocity was varied while keeping the injection hole diameter constant to verify whether the overall observations regarding flame stabilisation remain consistent. The results, shown in Fig. 3 of the Supplementary Material, exhibit similar trends. Specifically, flame lift-off is observed at the highest J ($d_i = 0.5$ mm), flame pinch-off occurs at the medium J ($d_i = 0.7$ mm), and a fully attached flame is seen at the injection location for the lowest J ($d_i = 1$ mm), consistent with the results presented in this section.

The distinct flame stabilisation behaviours observed in the experiments are interpreted through an LES study presented in the following section.

4. Large eddy simulation

The LES of the JICF configuration is carried out using Siemens Simcenter STARCCM+ software [21]. The simulation is first run to obtain well-converged Reynolds Averaged Navier Stokes (RANS) solutions to initialise the flow field from which the LES calculations are then performed. The LES employs adaptive mesh refinement, capturing approximately 90% of the turbulent kinetic energy. The simulation is advanced for a physical time of 120 ms, corresponding to 12 flow-through times, to ensure statistically meaningful time averaging. The flame is resolved using species transport coupled with a complex chemistry model. Rather than prescribing a single Lewis number, STARCCM+ solves the transport equations using specific mass diffusion

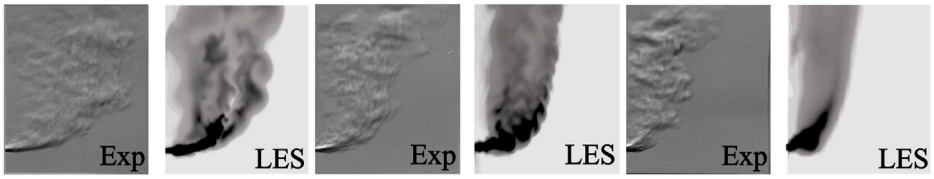

(a) $J = 314$ **(b)** $J = 82$ **(c)** $J = 20$

Fig. 4. Comparison of instantaneous experimental (Exp) schlieren images with numerical (LES) schlieren extracted from a section passing through the jet centreline.

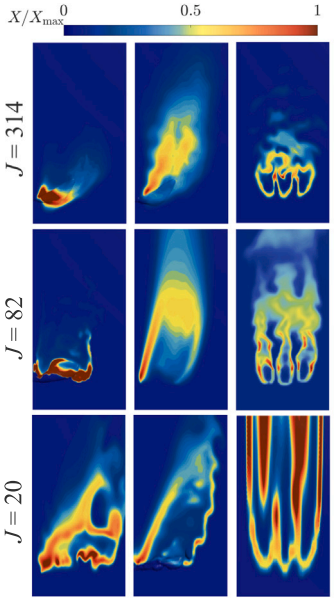

Fig. 5. Averaged heat release rate (left), OH mass fraction side view (middle), and OH mass fraction front view (right) from LES. The contours are extracted from a sectional cut passing through the jet centreline. All values are normalised with their respective maximum.

models. The software does not take the Lewis number as a direct input, but it accounts for the relevant transport properties to represent the underlying mass and energy diffusion processes. More details on the CFD methodology are provided in the Supplementary Material.

4.1. LES comparison with experiments

Firstly, cold flow schlieren images obtained using helium are compared with those of the CFD simulations. Numerical schlieren images represent sectional cuts at the jet centreline, whereas experimental schlieren images capture the integrated effect across the entire chamber. It can be seen from Fig. 4 that for all three cases, the evolution of the helium jet predicted from CFD simulations closely aligns with the experimental schlieren images. The jet angle relative to its axis, obtained from numerical schlieren, is 14° at $J = 340$, 22° at $J = 0.7$, and 27° at $J = 20$, closely matching the experimental schlieren measurements reported in Section 3.1 (16°, 18° and 31°, respectively). This indicates that the LES accurately predicts jet penetration trends consistent with the experiments. Further, the LES also clearly captures the jet stem distance and jet penetration length at various momentum flux ratios, along with correctly representing the trends observed as J is decreased. The flame front experimentally captured using the OH* chemiluminescence imaging is then compared against the OH mass fraction and heat release rate obtained from LES, which are shown in Fig. 5. It is important to note that OH* chemiluminescence and OH mass fraction are not expected to be the same, as the kinetic pathways for their formation are generally different [22] and hence are only qualitatively compared. In addition, OH may be a long-lived post-flame species while OH* marks the heat release zone. Fig. 5 shows the side view of the averaged heat release rate (left) along with the side and front views of the OH mass fraction (centre and right) from LES. The contours are taken from a cross-sectional plane through the jet centre.

From the figure, it can be seen that LES captures the general experimental trends well. More importantly, at the highest momentum flux ratio of $J = 314$, both the heat release rate and OH mass fraction capture the partial flame lift-off on the windward side that is observed on the experimental OH* chemiluminescence image shown in Fig. 3 (bottom-left, indicated by an arrow). It is worth noting that Fig. 3 presents line-of-sight integrated OH* chemiluminescence intensities from experiments, whereas Fig. 5 shows a cut-section view from LES. Since a cut-section view cannot be obtained experimentally, and the flame cannot be assumed to be axisymmetric in this case, the Abel transformation cannot be applied to reconstruct planar flame shape information. Consequently, only a qualitative comparison between Figs. 3 and 5 is possible.

At $J = 82$, the flame stabilisation is improved, and the minor flame pinch-off observed in the experiments (Fig. 3 bottom-centre) is captured on the heat release rate field from LES and seen as a minor lift-off on the OH mass fraction field (see side view). At the lowest momentum flux ratio of $J = 20$, the flame is attached to the inner wall, which can be seen on the OH mass fraction field from the LES.

Fig. 5 right shows the instantaneous OH mass fraction field with the front view of the jets. As the momentum flux ratio is decreased, it can be seen from both the OH mass fraction and the heat release rate fields that the flames become longer. This trend was also observed in the chemiluminescence images shown in Fig. 3 (top row). Further, it was seen from the experiments that the flame-to-flame interaction is more pronounced close to the tip at the highest momentum flux ratio (see Fig. 3 top-left), which is also captured in the OH mass fraction field of LES (see Fig. 5 top-right) where the flames touch each other close to the tip. The OH mass fraction field (bottom-right) at the lowest momentum flux ratio $J = 20$ shows noticeable interaction between the adjacent OH fields along the entire length, which is captured as a broad interaction of the outer flame boundary in the averaged chemiluminescence image in Fig. 3 (top-right).

Although the comparison between numerical simulations and experiments here is qualitative, the LES clearly captures the experimental trends well. Particle image velocimetry (PIV) and OH-planar laser-induced fluorescence (PLIF) studies are planned as future work to provide detailed quantification of the velocity field, OH distributions, strain rates and flame surface density at the different momentum flux ratios.

5. Discussion

Fig. 6 shows a side view of instantaneous velocity streamlines (normalised with a reference velocity) with an embossed isosurface of fuel at stoichiometry obtained from the LES at different momentum flux ratios. The isosurface is shown with an arrow on the rightmost figure

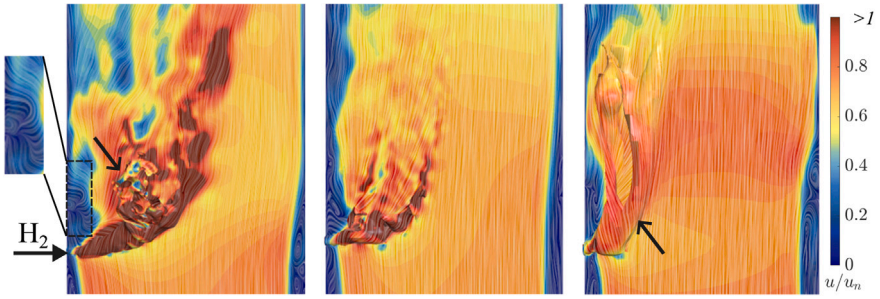

Fig. 6. Instantaneous velocity streamlines and magnitude (normalised) along with isosurface of fuel at stoichiometry (shown by black arrow) at the different momentum flux ratios.

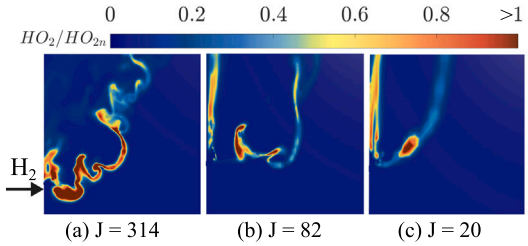

Fig. 7. Instantaneous mole fraction contours of perhydroxyl radical at different momentum flux ratios.

and is only faintly visible near the jet exit in the other two figures. At the highest momentum flux ratio shown on the left, it can be seen that the jets exit with a very high velocity. This results in higher penetration of the jet into the crossflow, as also seen in the experimental schlieren images in Fig. 2 (top row). On the downside, the higher momentum carried by the hydrogen jet results in lower initial mixing along the jet stem. The high jet velocity and poor mixing lead to the lift-off of the flame near the exit on the windward side (see Fig. 5 for lift-off). In addition, the higher jet velocity on the windward side, combined with stronger velocity gradients between the jet and crossflow seen in Fig. 6a (red-to-yellow ripples below the jet boundary on the windward side), would result in a higher strain rate in this region. This postulation aligns with Steinberg et al. [6], who reported a strong correlation between strain rate and the leading edge of the lifted flame branch, with the flame stabilising immediately downstream of the high strain rate region.

On the other hand, it can be observed that, on the leeward side, recirculation zones (marked with a black rectangle) are formed with the aid of the wake vortices due to the "bluff-body" effect of the jet stem. This low-velocity region likely results in the trapping of hydrogen and air and potentially some products, including free radicals, from the nearby reaction zone. The mole fraction contours of the perhydroxyl radical, which plays a crucial role in the chain branching reaction in hydrogen combustion [23], are shown in Fig. 7. The strong presence of HO_2 radical can be observed at $J = 314$ on the leeward side of the fuel jet, just above the injection location, confirming that the presence of a larger pool of radicals might indeed be responsible for the flame attaching to the leeward side. On the other hand, at lower momentum flux ratios, the LES predict that the HO_2 radicals are convected downstream by the large vertical velocity components likely formed in the wake recirculation zones, unable to collect on the leeward side of the jet exit.

Downstream of the jet, several small-scale velocity structures are observed (see black arrow in Fig. 6a), possibly due to strong shear layer vortices and wake vortices produced from the bluff-body effect of the jet stem, leading to intense mixing of the hydrogen with air. The existence of wake vortices (downstream of the black jet-core) can also be observed in the numerical schlieren shown in Fig. 4a. The presence of intense mixing in this region is also confirmed by the presence of a short fuel isosurface at stoichiometry, which can only be seen very close to the injection location and is absent downstream of the jet. Due to the rigorous and fast mixing achieved downstream of the jet, no fuel is expected further downstream of the chamber, thus establishing a compact flame. This was earlier seen in the chemiluminescence image (Fig. 3, bottom-left), where the flame front is more compact compared to lower momentum flux ratios.

When the momentum flux ratio is decreased to $J = 82$, there is still a short high-velocity region at the exit of the injection location and potentially high strain rates, which might result in a slight lift-off tendency. This is seen in the chemiluminescence image (Fig. 3 bottom-centre) as a minor pinch-off, but it is not as prominent as in the highest J case. Further downstream of the jet, ripples in the velocity field can also be observed, which are likely caused by the horseshoe vortices wrapping the incoming jets. The small-scale turbulent structures are not as prominent as in the highest J case, and hence the mixing would not be as vigorous.

At the lowest momentum flux ratio of $J = 20$, the velocity at the jet exit is comparatively lower in magnitude, causing flame stabilisation close to the injection location. It can also be seen that the isosurface of stoichiometry extends much longer compared to the other two cases, indicating that the mixing is slower in this case. This is expected as the intense turbulence structures, observed at the higher momentum flux ratios, are absent in this case, leading to reduced mixing. The mixing of fuel and air occurs further downstream along the chamber close to the inner wall, as indicated by the fuel isosurface. This results in a longer flame front that remains in closer proximity to the inner wall (see Fig. 3 bottom-right). It is also interesting to note that the velocity magnitudes downstream in the chamber are comparatively higher in the lower J case. This suggests that the jet behaves like a "bluff-body", reducing the effective crossflow area and thereby causing an increase in velocity. Further downstream, the influence of the bluff-body effect diminishes, and thus, there is no increase in the crossflow velocity (yellow region downstream of the jet). At the same momentum flux ratio, the wake length is expected to increase with jet diameter [24].

The experimentally validated LES provides further understanding of the flame stabilisation behaviour observed across different momentum flux ratios. The insights from this combined experimental–numerical approach offer a useful foundation for the design of combustors operating with pure hydrogen.

6. Conclusions

This work discusses the varied flame dynamics associated with a reactive jet in crossflow (JICF) configuration operating with hydrogen as fuel. In the first step, experiments are carried out under non-reactive conditions with helium as a surrogate to visualise the flow, followed

by high-speed chemiluminescence imaging performed under reactive conditions to visualise the flame. Three different hole diameters (0.5, 0.7 and 1 mm) are used with the aim of widely varying the JICF momentum flux ratio. In the second step, results from the experiments are compared with a large eddy simulation (LES) performed using STARCCM+, which is seen to qualitatively capture the experimental trends. The following conclusions are drawn on the basis of the joint experimental–numerical analysis of the results:

- At the highest momentum flux ratio, the spatially varying chemiluminescence intensity indicates a partial lift-off of the flame front on the windward side but a marginally attached flame on the leeward side. From the LES velocity field, the velocity magnitude of the jet is significantly high at the exit of the injection location. Further, the schlieren images obtained in the experiments show less intense mixing along the initial jet stem. The combined effect of higher jet velocity and reduced initial mixing led to flame lift-off on the windward side.
- Instantaneous velocity streamlines show a recirculation zone on the leeward side formed with the help of wake vortices. LES shows the trapping of free radicals in this region, such as HO_2, formed from the adjacent reaction region along with some hydrogen and air. This leads to the observed marginal flame stabilisation on the leeward side.
- The LES velocity field at the highest momentum flux ratio reveals several small-scale turbulent structures potentially formed and shed by the strong shear layer vortices. This leads to a rigorous and nearly complete mixing of hydrogen and air immediately downstream of the jet, establishing a short flame. The higher penetration leads to the jet expanding laterally, leading to the flames interacting at their tip.
- When the momentum flux ratio is reduced, the velocity of the jet is commensurately lower, causing the flame to stabilise closer to the injection holes. The schlieren image illustrates the jet bending shortly after entering the chamber, attributed to its reduced momentum. LES reveals the absence of intense turbulent structures, indicating reduced mixing. The fuel and air mix gradually downstream along the inner wall, resulting in a longer flame front.

This comprehensive joint experimental and numerical study on multiple jets in crossflow has provided valuable insights into various flame stabilisation mechanisms, serving as a potential guide for the development of practical fuel injection systems for hydrogen-burning engine configurations.

Novelty and significance

This study provides fundamental insights into the mechanisms of flame stabilisation in pure hydrogen jet in crossflow (JICF) flames, a configuration with practical relevance in low-carbon combustion systems. The novelty lies in the systematic exploration across a wide range of momentum flux ratios, including an order-of-magnitude higher values compared to existing literature, closing a critical gap in our current understanding. Additionally, this work considers a multi-JICF configuration allowing for the study of the effect of flame-to-flame interaction, an aspect not previously explored well in such configurations. These findings are significant to advancing the fundamental understanding of hydrogen combustion and can also serve as a practical foundation for designing fuel injection systems in engines operating with pure hydrogen.

CRediT authorship contribution statement

Preethi Rajendram Soundararajan: Writing – review & editing, Writing – original draft, Visualization, Validation, Methodology, Investigation, Formal analysis, Data curation, Conceptualization. **Pierre Q. Gauthier:** Writing – original draft, Visualization, Investigation, Formal analysis, Data curation. **Peter J. Benie:** Software, Data curation. **Epaminondas Mastorakos:** Writing – review & editing, Supervision, Project administration, Funding acquisition, Conceptualization.

Declaration of competing interest

The authors declare that they have no known competing financial interests or personal relationships that could have appeared to influence the work reported in this paper.The author is an Editorial Board Member/Editor-in-Chief/Associate Editor/Guest Editor for this journal and was not involved in the editorial review or the decision to publish this article.

Acknowledgements

PRS & EM acknowledge the funding received from the Horizon Europe Research and Innovation Program HESTIA under grant agreement no. 101056865. PRS acknowledges the support of Mr. Luke Arnold, University of Cambridge, for the design and fabrication of the experimental setup. PRS is thankful to Dr. Pedro M. de Oliveira for initial discussions on the JICF setup. The views expressed here do not represent those of the European Commission.

Appendix A. Supplementary data

Supplementary material related to this article can be found online at https://doi.org/10.1016/j.proci.2025.105929.

References

[1] Advisory Council for Aviation Research and Innovation in Europe (ACARE), Fly the green deal, 2022.
[2] A.R. Karagozian, Transverse jets and their control, Prog. Energy Combust. Sci. 36 (2010) 531–553.
[3] K. Mahesh, The interaction of jets with crossflow, Ann. Rev. Fluid Mech. 45 (2013) 379–407.
[4] A.R. Karagozian, The jet in crossflow, Phys. Fluids 26 (2014).
[5] R.F. Huang, S.M. Wang, Characteristic flow modes of wake-stabilized jet flames in a transverse air stream, Combust. Flame 117 (1–2) (1999) 59–77.
[6] A.M. Steinberg, R. Sadanandan, C. Dem, P. Kutne, W. Meier, Structure and stabilization of hydrogen jet flames in cross-flows, Proc. Combust. Inst. 34 (1) (2013) 1499–1507.
[7] H. Kolla, R.W. Grout, A. Gruber, J.H. Chen, Mechanisms of flame stabilization and blowout in a reacting turbulent hydrogen jet in cross-flow, Combust. Flame 159 (8) (2012) 2755–2766.
[8] P. Saini, I. Chterev, J. Pareja, M. Aigner, I. Boxx, Effects of hydrogen-enrichment on flame-holding of natural gas jet flames in crossflow at elevated temperature and pressure, Flow, Turb. Combust. 107 (1) (2021) 219–243.
[9] A.B. Murugavel, J.C. Massey, N. Swaminathan, Pressure effects on mixing and combustion mode of a hydrogen/helium jet in cross-flow, J. Fluid Mech. 1017 (2025) A3.
[10] B.D. Pratte, W.D. Baines, Profiles of the round turbulent jet in a cross flow, J. Hydraul. Div. 93 (6) (1967) 53–64.
[11] A. Oamjee, R. Sadanandan, Suitability of helium gas as surrogate fuel for hydrogen in H2-air non-reactive supersonic mixing studies, Intl. J. Hydrog. Energy 47 (15) (2022) 9408–9421.
[12] A.B. Murugavel, J.C. Massey, Y. Tanaka, N. Swaminathan, The effect of methane addition on reacting hydrogen jets in crossflow, Int. J. Hydrog. Energy 80 (2024) 57–67.
[13] V. Nair, M. Sirignano, B.L. Emerson, T.C. Lieuwen, Combustion and flame position impacts on shear layer dynamics in a reacting jet in cross-flow, J. Fluid Mech. 942 (2022) A41.
[14] I. Hurle, R. Price, T.M. Sugden, A. Thomas, Sound emission from open turbulent premixed flames, Proc. R. Soc. Ser. A. Math. Phys. Sci. 303 (1475) (1968) 409–427.
[15] F.G. Schiavone, A. Aniello, E. Riber, T. Schuller, D. Laera, On the adequacy of OH* as heat release marker for hydrogen–air flames, Proc. Combust. Inst. 40 (1–4) (2024) 105248.
[16] T. Fric, A. Roshko, Vortical structure in the wake of a transverse jet, J. Fluid Mech. 279 (1994) 1–47.
[17] J.P. Bons, R. Sondergaard, R.B. Rivir, The fluid dynamics of LPT blade separation control using pulsed jets, J. Turbomach. 124 (1) (2002) 77–85.
[18] S.V. Ekkad, S. Ou, R.B. Rivir, Effect of jet pulsation and duty cycle on film cooling from a single jet on a leading edge model, J. Turbomach. 128 (2006) 564–571.
[19] K. Javadi, M. Taeibi-Rahni, M. Darbandi, Jet-into-crossflow boundary-layer control: innovation in gas turbine blade cooling, AIAA J. 45 (12) (2007) 2910–2925.

[20] J.D. Holdeman, Mixing of multiple jets with a confined subsonic crossflow, Prog. Energy Combust. Sci. 19 (1) (1993) 31–70.
[21] Siemens star-CCM user guide theory, in: Star-CCM+, IOP Publishing, Consulted 2019-10-2024.
[22] T. Paschal, P. Parajuli, M.A. Turner, E.L. Petersen, W.D. Kulatilaka, High-speed OH* and CH* chemiluminescence imaging and OH planar laser-induced fluorescence (PLIF) in spherically expanding flames, in: AIAA Scitech 2019 Forum, 2019, p. 0574.
[23] M.A. Mueller, R.A. Yetter, F.L. Dryer, Measurement of the rate constant forH+O2+M → HO2+ M (M=N2, Ar) using kinetic modeling of the high-pressure H2/O2/NOx reaction, in: Symp. (Int.) Combust., vol. 27, (1) Elsevier, 1998, pp. 177–184.
[24] A. Roshko, Experiments on the flow past a circular cylinder at very high Reynolds number, J. Fluid Mech. 10 (3) (1961) 345–356.